Chapter 14
Reconciling the Difference Between Test and Real Environments: Improving Fixture Design Based on Modal Strain

Scott A. Smith and Matthew R.W. Brake

Abstract With the recent push to make automobiles, aircraft, and other vehicles more fuel-efficient, the redesign of many components are currently underway to reduce the conservativeness of the design with an intent to reduce weight. Laboratory tests are performed to speed up the design qualification process. However, the fixtures used are typically rigid, which provides insight into how a component responds and fails in a "'fixed" base manner. Laboratory tests need to be able to reproduce the same stresses and strains experienced to represent real environments. This work proposes that a fixture mimicking the local stiffness and dynamics is required to emulate the actual environmental conditions. This work postulates that the local modal displacements and strains need to match these local dynamics, and the best way to achieve this is through a truncated system.

Keywords Boundary conditions · BARC · Fixture design · Dynamic matching · Component testing

14.1 Approach

To investigate this theory, a simple Euler-Bernoulli beam model is truncated and spring-mass systems are attached at the boundaries. Parameters for the spring-masses are optimized to match the first bending mode dynamics of the truncated and full beams. The full beam is assumed to be the actual environment and is given as the analytical expression of a free-free Euler-Bernoulli Beam of length $5L$, given in Eq. 14.1 and shown in Fig. 14.1a. A truncated beam of length L with attached spring-mass systems (Fig. 14.1b) is utilized as the representative system. For this system Eqs. 14.1a and 14.1b with the appropriate length of L are the same, and Eq. 14.1c is modified to those given in Eq. 14.2. The beams are taken to have the following properties: Modulus of Elasticity of 69 GPa, Density of 2700 $^{\mathrm{kg}}/_{\mathrm{m}^3}$, and a 2 cm square cross-section.

$$\frac{\partial^2}{\partial x^2}\left(-EI\frac{\partial^2 w(x,t)}{\partial x^2}\right) = \rho A\frac{\partial^2 w(x,t)}{\partial t^2}, \quad x \in [0, 5L] \tag{14.1a}$$

$$\frac{\partial^2 w(x,t)}{\partial x^2} = 0, \quad x \in \{0, 5L\} \tag{14.1b}$$

$$\frac{\partial^3 w(x,t)}{\partial x^3} = 0, \quad x \in \{0, 5L\} \tag{14.1c}$$

$$-EI\frac{\partial^3 w(0,t)}{\partial x^3} = F_1 = kz_0(t) \tag{14.2a}$$

$$-EI\frac{\partial^3 w(L,t)}{\partial x^3} = -F_2 = -kz_L(t) \tag{14.2b}$$

S. A. Smith (✉) · M. R. W. Brake
William Marsh Rice University, Houston, TX, USA
e-mail: scott.a.smith@rice.edu; brake@rice.edu

D. S. Epp (ed.), *Special Topics in Structural Dynamics & Experimental Techniques, Volume 5*, Conference Proceedings of the Society for Experimental Mechanics Series, https://doi.org/10.1007/978-3-030-47709-7_14

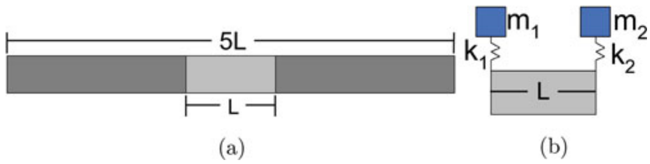

Fig. 14.1 Euler-Bernoulli beams studied; (**a**) full length and (**b**) truncated with spring-masses attached at the boundaries

F_1 and F_2 are solved by performing force balance at the boundaries in Fig. 14.1b. The equation of motion for the boundary condition is given as:

$$M\frac{d^2 z_x}{dt^2} = k\left(\Theta(x) - z_x\right) \tag{14.3}$$

Using Eqs. 14.3 and 14.2, and applying separation of variables, the steady state boundary becomes

$$-EI\frac{d^3\Theta(0)}{dx^3} = \frac{\omega^2 M_1 k_1 \Theta(0)}{M_1\omega^2 - k_1} \tag{14.4a}$$

$$-EI\frac{d^3\Theta(L)}{dx^3} = -\frac{\omega^2 M_2 k_2 \Theta(L)}{M_2\omega^2 - k_2} \tag{14.4b}$$

Using Eqs. 14.1a, 14.1b, and 14.4 the natural frequencies and mode shapes can be found as:

$$\begin{aligned} &2\cos\beta L\cosh\beta L - 2K_1\cos\beta L\sinh\beta L + 2K_1\sin\beta L\cosh\beta L \\ &-2K_2\cos\beta L\sinh\beta L + 2K_2\sin\beta L\cosh\beta L - 4K_1K_2\sin\beta L\sinh\beta L = 0 \end{aligned} \tag{14.5a}$$

$$\beta^4 = \omega^2\frac{\rho A}{EI} \tag{14.5b}$$

$$\Theta_L(x) = A\left[\sin(\beta x) + \frac{1-\Psi}{2K_1}\cos(\beta x) + \Psi\sinh(\beta x) + \frac{1-\Psi}{2K_1}\cosh(\beta x)\right] \tag{14.5c}$$

$$\Psi = \frac{\cos(\beta L) + K_2\sin(\beta L) - \frac{\sigma}{2K_1}}{\cosh(\beta L) - K_2\sinh(\beta L) - \frac{\sigma}{2K_1}} \tag{14.5d}$$

$$\sigma = \sin(\beta L) - K_2\cos(\beta L) + \sinh(\beta L) - K_2\cosh(\beta L) \tag{14.5e}$$

$$K_1 = \frac{\beta m_1}{\rho A\left(\frac{m_1}{k_1}\beta^4\frac{EI}{\rho A} - 1\right)} \tag{14.5f}$$

$$K_2 = \frac{\beta m_2}{\rho A\left(\frac{m_2}{k_2}\beta^4\frac{EI}{\rho A} - 1\right)} \tag{14.5g}$$

14.2 Simulations

To optimize the springs and masses, an implementation of NSGA-II in Matlab's global optimization toolbox is utilized. The program is used to optimize the scaled mode shape (Eq. 14.6) or strain mode shape (Eq. 14.7) using the Modal Assurance Criterion (MAC), Eq. 14.8, or Modal Strain Assurance Criterion (MSAC) when strain mode shape is used; and the relative error between the frequency of the truncated beam to full length beam.

$$\Theta_s = \frac{\Theta - \min(\Theta)}{\max(\Theta) - \min(\Theta)} \tag{14.6}$$

$$\Psi = \frac{d\Theta}{dx} \tag{14.7}$$

$$MAC = \frac{\left|\Theta'_L \Theta_{5L}\right|^2}{\left(\Theta'_L \Theta_L\right)\left(\Theta'_{5L} \Theta^*_{5L}\right)} \tag{14.8}$$

Two cases are analyzed, symmetric (SSM) and asymmetric (ASM) spring-masses. The symmetric case is studied because the truncated beam is assumed to be centered in the whole beam. The Pareto fronts from using the two different shapes are shown in Fig. 14.2a, b. The asymmetric case allows for the springs and masses to vary independently, the Pareto fronts are shown in Fig. 14.2c, d. As ASM did not converge to a reasonable error for frequency (minimum achieved was 120%) the results from the symmetric cases were used to seed the first generation, the results are shown in Fig. 14.2e, f.

14.3 Conclusions

The conclusion of this study is that there is a possibility to truncate boundary conditions such that the dynamics seen by a component can be matched. However, the use of optimization techniques need to be surveyed in more detail. Furthermore, the applicability of other techniques such as transmission simulator or effective mass need to be assessed. These methods, though, tend to return non-physical masses and stiffness matrices. Since, the overall goal is to make a fixture for testing, the parameters need to have physical representatives. The method must be expanded to a 3D finite element model of a beam, so that it may be applied to more complex structures such as the Box Assembly with Removable Component.

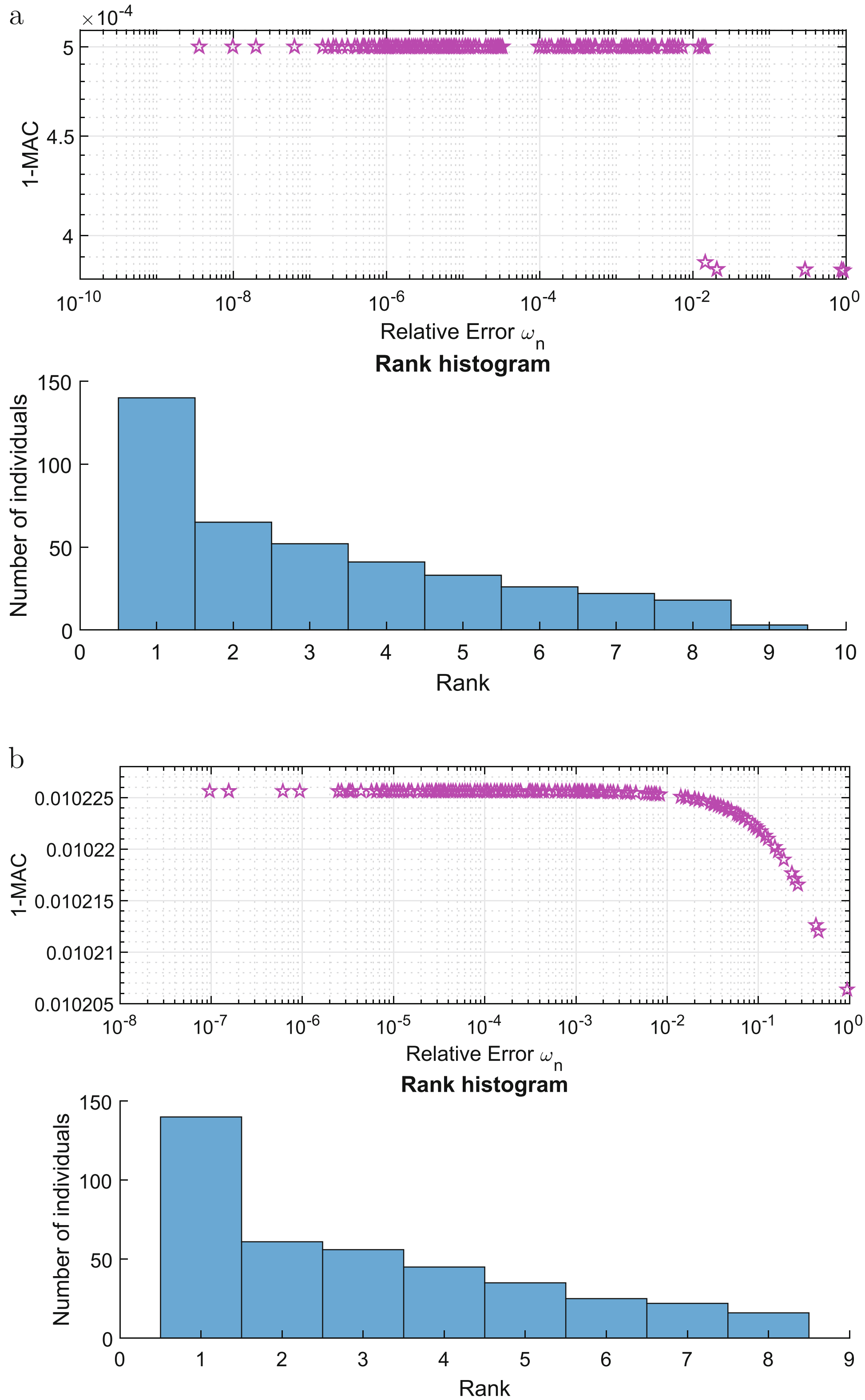

Fig. 14.2 Pareto front and rank histograms of SSM (**a**) scaled and (**b**) strain mode shapes, ASM for (**c**) scaled and (**d**) strain mode shapes, and ASM seeded with SSM for (**e**) scaled and (**f**) strain mode shapes

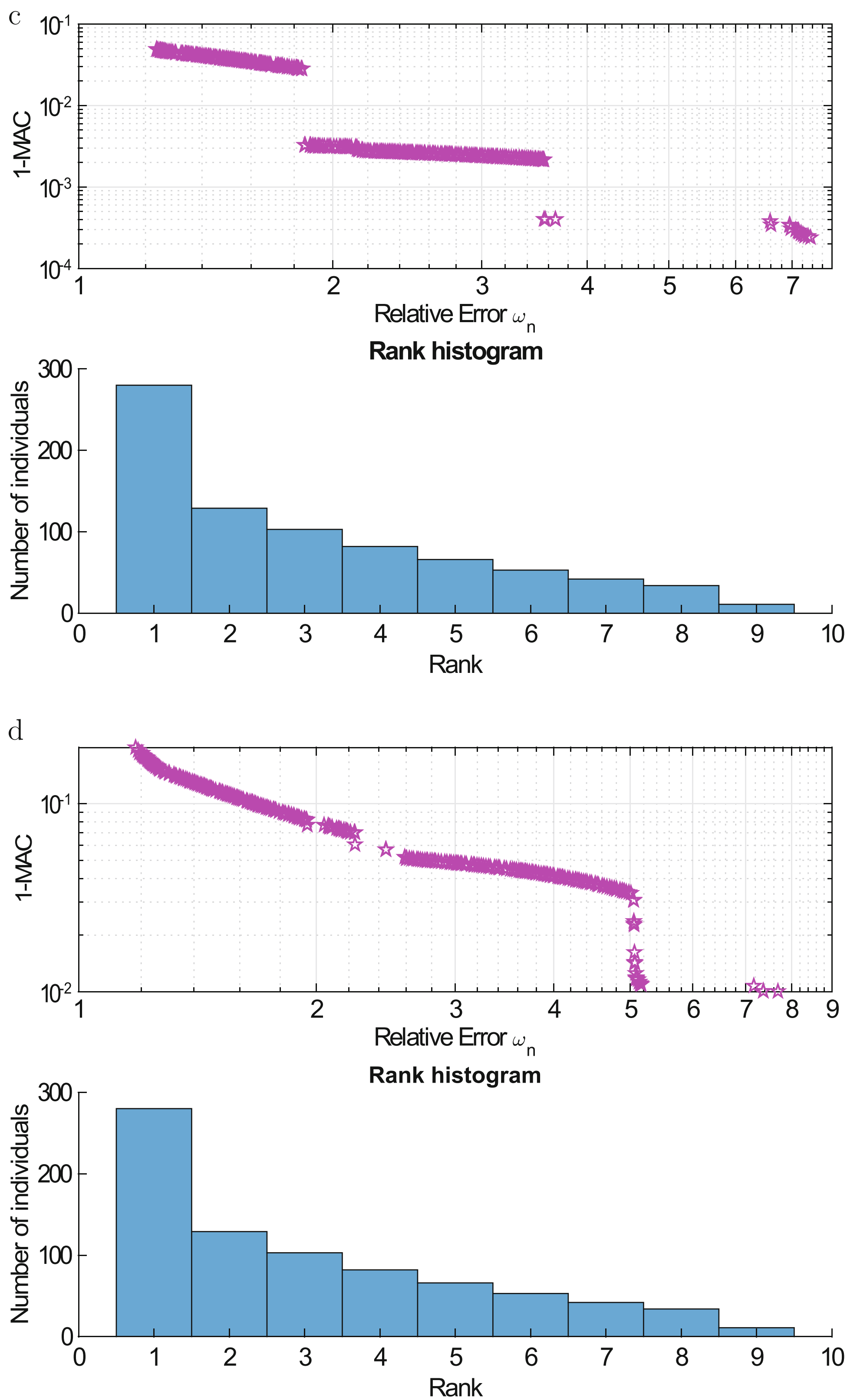

Fig. 14.2 (continued)

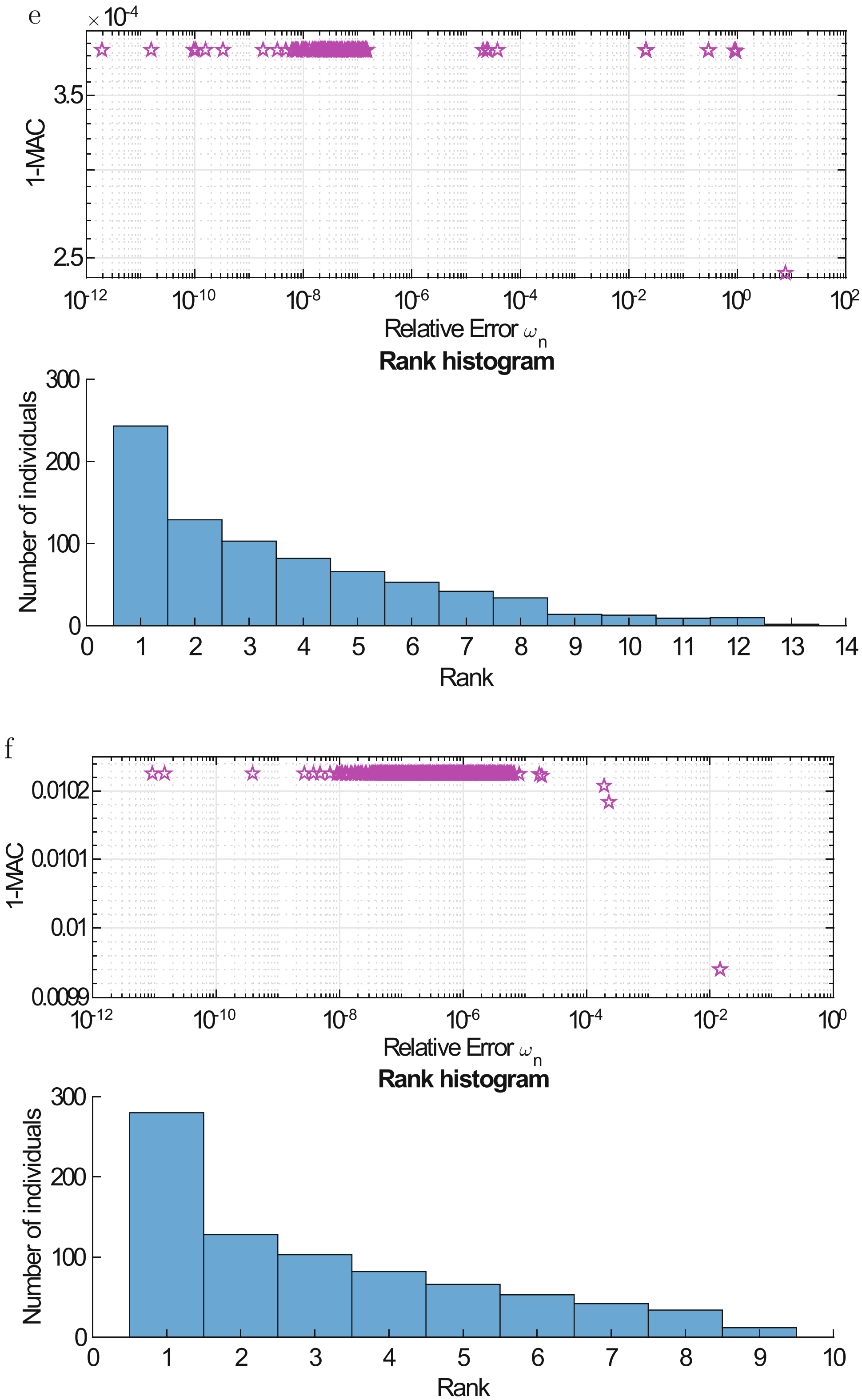

Fig. 14.2 (continued)

References

1. Soine, D.E., Jones, R.J. Jr., Harvie, J.M., Skousen, T.J., Schoenherr, T.F.: Designing hardware for the boundary condition round robin challenge. In: 36th International Modal Analysis Conference (IMAC XXXVI), Orlando (2018)
2. Schoenherr, T.F.: Derivation of six degree of freedom shaker inputs using sub-structuring techniques (2018)
3. Dilworth, B.J., Karlicek, A., Thibault, L.: An approach to component testing: an analytical study (2019)
4. Ristow, J., Gray, J.: Comparing fixed-base and shaker table model correlation methods using JIM beam (2019)
5. Rohe, D.P., Schultz, R.A., Schoenherr, T.F., Skousen, T.J., Jones, R.J.: Comparison of multi-axis testing of the barc structure with varying boundary conditions (2019)
6. Schoenherr, T.F., Coffin, P., Clark, B.: Use of topology optimization to design shock and vibration test fixtures (2019)
7. Hall, T.M.: Analytically investigating impedance-matching test fixtures (2019)
8. Zwink, B., Avitable, P., Tipton, D.G.: Modal projection matching (2019)
9. Devine, T.A., Malladi, V.S., Tarazaga, P.A.: Replicating responses: a virtual environmental test of unknown boundary conditions (2019)
10. Mayes, R., Andkers, L., Daborn, P.: Predicting system response at unmeasured locations (2019)
11. Mayes, R., Andkers, L., Daborn, P., Moulder, T., Ind, P.: Optimization of shaker locations for multiple shaker environmental testing (2019)
12. Harvie, J.M., van der Seijs, M.: Application of transfer path analysis techniques to the boundary condition challenge problem (2019)
13. Schultz, R.: A demonstration of force estimation and regularization methods for multi-shaker testing (2019)
14. Rohe, D.P., Nelson, G.D., Schultz, R.A.: Strategies for shaker placement for impedance-matched multi-axis testing (2019)
15. Musella, U., Blanco, M.A., Mastrodicasa, D., Monco, G., Lorenzo, E.D., Manzato, S., Peeters, B., Mucchi, E., Guillaume, P.: Combining test and simulation to tackle the challenges derived from boundary conditions mismatches in environmental testing (2019)
16. Devine, T.A., Malladi, V.S., Tarazaga, P.A.: Electromechanical impedance method for applications in boundary condition replication (2019)
17. Reyes, J.M., Avitabile, P., Jones, R., Soine, D.: Fixture neutralization method – adjustment of vibration response to account for fixture-test article dynamic coupling effects using measured frequency response functions (2019)
18. Reyes, J.M., Avitabile, P.: Implementation of the fixture neutralization methodology using data physics vibration controller (2019)